Engineering the Substrate Specificity and Reactivity of a Heme Protein: Creation of an Ascorbate Binding Site in Cytochrome *c* Peroxidase[†]

Emma J. Murphy,[‡] Clive L. Metcalfe,[‡] Jaswir Basran,[§] Peter C. E. Moody,[§] and Emma Lloyd Raven[‡,*]

Department of Chemistry, Henry Wellcome Building, University of Leicester, University Road, Leicester, LE1 9HN, England U.K., and Department of Biochemistry and Henry Wellcome Laboratories for Structural Biology, Henry Wellcome Building, University of Leicester, Lancaster Road, Leicester, LE1 9HN, England U.K.

Received August 6, 2008; Revised Manuscript Received November 7, 2008

ABSTRACT: The binding of substrates to heme enzymes has been widely assumed to occur at the so-called δ-heme edge. Recently, however, a number of examples have appeared in which substrate binding at an alternative site, the γ-heme edge, is also possible. In previous work [Sharp et al. (2003) *Nat. Struct. Biol. 10*, 303−307], we showed that binding of ascorbate to ascorbate peroxidase occurred at the γ-heme edge. Here, we show that the closely related cytochrome *c* peroxidase enzyme can duplicate the substrate binding properties of ascorbate peroxidase through the introduction of relatively modest structural changes at Tyr36 and Asn184. Hence, crystallographic data for the Y36A/N184R/W191F triple variant of cytochrome *c* peroxidase shows ascorbate bound to the γ-heme edge, with hydrogen bonds to the heme propionate and Arg184. In parallel mechanistic studies in variants incorporating the W191F mutation, we show that a transient porphyrin π-cation radical in Compound I of cytochrome *c* peroxidase, analogous to that observed in ascorbate peroxidase, is competent for ascorbate oxidation but that under steady state conditions this intermediate decays too rapidly to sustain efficient turnover of ascorbate. The results are discussed in terms of our more general understanding of substrate oxidation across other heme proteins, and the emerging role of the heme propionates at the γ-heme edge.

Our understanding of substrate binding across various heme enzymes developed largely from crystallographic information for a number of heme peroxidase enzymes. The first structures to appear showed binding of aromatic substrates close to the so-called δ-heme edge (*1*−*5*), and these structures were consistent with other observations, for example from earlier chemical modification work (*6*−*8*), in which substrate binding at the δ-heme edge was also implicated. As a consequence, a consensus emerged in which substrate binding and oxidation at the so-called δ-heme edge was widely assumed. With the exception of the cytochrome *c* peroxidase/cytochrome *c* complex—which was known to be anomalous in part because of its unusual substrate—the only outlier to this general "trend" was the structure for the manganese peroxidase/Mn(II) complex, which showed Mn(II) bound at a different location, close to the γ-heme edge and ligated by carboxylate groups and the heme 6-propionate (*9*). Later on, two other structures appeared, for the ascorbate peroxidase/ascorbate (*10*) and nitric oxide synthase/tetrahydrobiopterin (*11, 12*) complexes. These structures also revealed hydrogen bonding interactions between the substrate and the heme 6-propionate at the γ-heme edge. It became clear, therefore, that substrate binding at the δ-heme edge was not the only means by which the enzyme and substrate might productively associate with one another. As far as the protein is concerned, this offers distinct advantages over the "one-site-fits-all" model, because it provides more than one route through which electron delivery can be channeled. Consequently, oxidation of different *types* of substrate can be accommodated within the *same* protein framework, for example in ascorbate peroxidase where (hydrophobic) aromatic substrates and (hydrophilic) ascorbate are oxidized at different sites (*1, 10*).

In previous work (*10*), we identified the ascorbate binding site in ascorbate peroxidase (APX[1]), Figure 1. The structure was helpful not only because it revealed the details of the binding interactions in APX but also because but also because it helped to rationalize differences with the closely related cytochrome *c* peroxidase enzyme. Hence, we noted that the residues required for ascorbate binding (Arg172, Lys 30, Figure 1 (inset)) are replaced by Asn184 and Asp33 in C*c*P; conversely, the residues required for binding of cytochrome *c* (Asp34, Glu35, Asp37, Glu290 (*13*)) are completely missing in APX. This comparison of the two structures also accounted for the observation that Trp179 is not essential for catalysis in APX (*14*) while the equivalent residue (Trp191) in C*c*P is (*15*), because in APX there is direct coupling of the substrate to the heme propionate, completely bypassing Trp179. In this work, we demonstrate that C*c*P can, with relatively modest changes in protein structure

[†] This work was supported by grants from the BBSRC (Project Grants BB/C00602X/1, BB/C001184/1 and IIP 0206 /009, and a studentship to E.J.M.).

* To whom correspondence should be addressed. Tel: +44 (0)116 2297047. Fax: +44 (0)116 252 2789. E-mail: emma.raven@le.ac.uk.

[‡] Department of Chemistry.

[§] Department of Biochemistry and Henry Wellcome Laboratories for Structural Biology.

[1] Abbreviations: APX, ascorbate peroxidase; C*c*P, cytochrome *c* peroxidase.

10.1021/bi801480r CCC: $40.75
Published on Web 12/05/2008

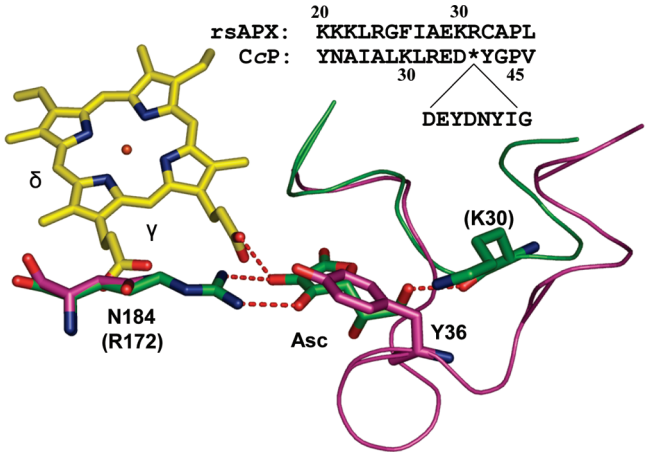

FIGURE 1: Comparison of APX with C*c*P, as described previously (*10*). The structure of the APX−ascorbate complex (PDB accession code 1OAF, in green) (*10*) overlaid with the structure of C*c*P (PDB accession code 2CYP in purple). The three main hydrogen bonding interactions between APX and ascorbate (Asc) are shown in red. C*c*P residues are indicated and those for APX given in parentheses. The δ- and γ-heme edges are indicated. The loop regions (APX residues 26−36 and C*c*P residues 28−45) are shown along with the side chain of Tyr36 in C*c*P which blocks the equivalent ascorbate binding site found in APX. Residues important for ascorbate binding in APX are also shown (K30, R172) along with the residue equivalent to R172 in C*c*P (N184). Inset: Structural alignment of APX and C*c*P in the region of the ascorbate binding site. The sequence from 34 to 41 is missing in APX and is replaced with a single arginine residue at position 31. Glu 290 is also missing in APX due to a C-terminal truncation. This figure was prepared using PyMol (*43*).

around Tyr36 and Asn184 (Figure 1), be re-engineered to bind and oxidize ascorbate at the γ-heme edge.

EXPERIMENTAL PROCEDURES

Materials. L-Ascorbic acid (Aldrich Chemical Co.) and buffers (Fisher) were all of the highest analytical grade (99%+ purity) and were used without further purification. Water was purified by an Elga purelab purification system and all buffers were filtered (0.2 μm) prior to use. Hydrogen peroxide solutions were freshly prepared by dilution of a 30% (v/v) solution (BDH): exact concentrations were determined using the published absorption coefficient (ε_{240} = 39.4 M^{-1} cm^{-1}) (*16*). All molecular biology kits and enzymes were used according to manufacturer's protocols.

Mutagenesis, Protein Expression and Purification. Site-directed mutagenesis on C*c*P was performed according to the Quikchange protocol (Stratagene Ltd., Cambridge, U.K.). Mutations were confirmed by DNA sequencing as reported previously (*17*). A number of single, double and triple variants of C*c*P were prepared involving Tyr36, Asn184 and Trp191. In total 7 variants were prepared: Y36A, N184R, W191F, Y36A/N184R, Y36A/W191F, N184R/W191F and Y36A/N184R/W191F.

Wild type C*c*P and all variants were prepared and isolated with modifications to published procedures (*18*). All variants containing the Y36A mutation failed to recrystallize against water as per the published procedure, and so further purification after gel filtration chromatography was carried out by FPLC (Superdex 75 gel filtration column), after which crystallization occurred. Absorption coefficients for all variants were determined using the pyridine-hemochromogen method (*19*) and are given in Table 1; the absorption coefficients of wild type C*c*P and W191F have been reported previously (*15, 18*).

Wavelength maxima for the ferric derivatives of all variants are given in Table 1. Wild type C*c*P and the single variants have spectra which are consistent with a predominantly high-spin heme species, either 5- or 6-coordinate with a water at the axial position. In contrast, the Y36A/W191F, Y36A/N184R and Y36A/N184R/W191F variants have similar spectra which are consistent with a predominantly low-spin heme species, as observed in the alkaline form of C*c*P (*20*). Spectra are shown in Figure S1 of the Supporting Information. For all variants, the crystal structures (below) show an oxygen ligand bound to the iron with Fe−O bond distances ranging between 2.15 and 2.87 Å. However, these distances do not correlate with the high-spin/low-spin distributions seen in the electronic spectra (i.e., expected longer bond lengths for high-spin species compared to low-spin) and we interpret these bond distances as arising from coordination of either water or hydroxide.

Protein Crystallography. Crystals were prepared by microdialysis with 100 μL of a 10−30 mg/mL solution of enzyme in 500 mM potassium phosphate, pH 6.0 against 10 mL of 50 mM potassium phosphate, pH 6.0 containing 30% 2-methyl-2,4-pentanediol by volume. With the exception of the triple variant, crystals were grown at 4 °C for approximately two days, yielding large red crystals. The triple variant needed up to two weeks to crystallize at 4 °C, and crystals were much smaller. For the structure of the Y36A/N184R/W191F−ascorbate complex, crystals were soaked in mother liquor containing 100 mM ascorbate for 5 min before rapid cooling to 100 K. Soaks at higher concentrations of ascorbate and for longer times caused the crystals to crack, and many variations of the soak (including variations in length of soak and ascorbate concentration) were attempted before the ascorbate bound structure was obtained. Although less than 50% of the unique data was collected, the presence of bound ascorbate was validated by difference Fourier calculations (discussed in Figure S3 of the Supporting Information).

Data Collection and Refinement. Diffraction data were collected for all variants in house using a Rigaku RU2HB X-ray generator with copper anode and Xenocs multilayer optics and an R-Axis IV detector. All data were collected at 100 K. Data were indexed, integrated and scaled using MOSFLM (*21*) and SCALA (*22*). Data collection statistics are shown in Table 2, and 5% of the data were flagged for the calculation of R_{free} and excluded from subsequent refinement. The structures were refined from the 1.70 Å wild type C*c*P structure (*23*) (Protein data bank entry 2CYP). All refinement used REFMAC5 (*24*) from the CCP4 suite (*22*). Calculation of difference Fourier maps showed clear and unambiguous electron density for bound ascorbate in the Y36A/N184R/W191F structure. Ascorbate was incorporated into the last cycles of refinement. COOT (*25*) was used throughout for manual adjustment, ligand fitting and interpretation of the water structure.

Steady State Kinetics. Steady-state measurements (100 mM potassium phosphate, pH 6.0, 25.0 °C) for ascorbic acid, guaiacol (2-methoxy phenol) and cytochrome *c* (horse heart, Sigma) were carried out according to published protocols (*26*−*28*). For L-ascorbic acid initial

Table 1: Wavelength Maxima (nm) for the Ferric Derivatives of the Variants Examined in This Work[a]

variant	wavelength maximum (nm)				
	soret	CT1	β	α	CT2
wild type C*c*P	408 (102)	506	544 (sh)	589 (sh)	647
N184R	408 (102)	507	544 (sh)	589 (sh)	644
Y36A	408 (104)	502	538 (sh)	585 (sh)	630
W191F	408 (109)	504	544 (sh)	589 (sh)	645
N184R/W191F	412 (99)		536	563 (sh)	645 (sh)
Y36A/W191F	414 (350 sh) (98)	485 (sh)	533	566	632 (sh)
Y36A/N184R	414 (354 sh) (96)	489 (sh)	534	568	620 (sh)
Y36A/N184R/W191F	414 (350 sh) (100)	489 (sh)	536	567	620 (sh)

[a] Absorption coefficients for the ferric derivatives (mM^{-1} cm^{-1}) are shown in parentheses. sh = shoulder.

Table 2: Data Collection and Refinement Statistics for the Variants Examined in This Work and for the Y36A/N184R/W191F−Ascorbate Complex[a]

protein	N184R	Y36A	W191F	N184R/ W191F	Y36A/ W191F	Y36A/ N184R	Y36A/N184R/ W191F	Y36A/N184R/ W191F−ascorbate complex
				Data Collection				
space group	$P2_12_12_1$	$P2_12_12_1$	$P2_12_12_1$	$P2_12_12_1$	$P2_12_12_1$	$P2_12_12_1$	$P2_12_12_1$	$P2_12_12_1$
unit cell (Å)								
A	51.0	51.1	51.1	51.0	51.0	51.1	51.0	51.0
B	74.5	75.8	75.3	74.6	75.0	75.1	74.5	74.4
C	106.3	107.1	106.3	106.7	106.4-	107.3	106.5	106.6
resolution (Å)	61.78−1.40 (1.48−1.40)	46.13- 2.01 (2.12−2.01)	27.16−1.80 (1.90−1.80)	27.17 −1.80 (1.90−1.80)	45.93−2.10 (2.21−2.10)	30.28−2.01 (2.11−2.01)	39.13 - 1.86 (1.96−1.86)	42.03- 2.01 (2.12−2.01)
total observations	411140 (31869)	58833 (8129)	74923 (6085)	87578 (8923)	196453 (27085)	38648 (4669)	120110 (16654)	15047 (2103)
unique reflections	80702 (11309)	26868 (3737)	29668 (3257)	34080 (4620)	24405 (3514)	18732 (2625)	31259 (4618)	12304 (1668)
$I/\sigma I$	15.6 (4.4)	15.2 (6.6)	22.9 (4.0)	18.7 (5.3)	9.1 (4.3)	15.1 (3.0)	18.0 (3.4)	17.3 (5.2)
R_{merge}	0.082 (0.275)	0.047 (0.112)	0.039 (0.218)	0.044 (0.125)	0.076 (0.298)	0.055 (0.389)	0.063 (0.271)	0.033 (0.104)
completeness (%)	98.9 (95.9)	95.0 (92.1)	76.8 (59.4)	88.8 (77.5)	99.7 (99.5)	65.8 (64.6)	90.4 (92.3)	45.9 (42.5)[b]
				Refinement Statistics				
R_{work}	0.172	0.161	0.174	0.186	0.168	0.165	0.169	0.187
R_{free}	0.193	0.203	0.214	0.216	0.210	0.201	0.205	0.246
RMSD								
bonds (Å)	0.007	0.015	0.012	0.013	0.015	0.014	0.013	0.013
angles (deg)	1.12	1.37	1.41	1.37	1.34	1.39	1.25	1.44

[a] Values in parentheses refer to the outer resolution bin. [b] Discussed in Figure S3 of the Supporting Information.

rates were calculated from time-dependent absorbance changes at 290 nm and multiplied by a factor of 2 to allow for disproportionation of the monodehydroascorbate radical (*26*). Substrate concentrations were calculated using the following absorption coefficients: L-ascorbic acid, $\varepsilon_{290} = 2.8$ mM^{-1} cm^{-1} (*29*); guaiacol, $\varepsilon_{470} = 22.6$ mM^{-1} cm^{-1} (*30*); cytochrome *c*, $\varepsilon_{550} = 27.7$ mM^{-1} cm^{-1}. Concentration ranges were 10−750 μM for ascorbate, 2 mM to 60 mm for guaiacol, and 5−200 μM for cytochrome *c*; the concentration of peroxide was 200 μM in all assays. Data were fitted to the Michaelis−Menten equation as previously described (*26, 28*).

Transient-State Kinetics. Transient-state kinetics were performed using a SX.18 MV stopped-flow spectrophotometer (Applied Photophysics Ltd.) in 100 mM potassium phosphate, pH 6.0 at 10 °C. Time-dependent spectral changes occurring upon reaction of C*c*P with H_2O_2 were monitored using a photodiode array detector and X-SCAN software (Applied Photophysics Ltd.). In these experiments the protein (2 μM) was mixed with either a stoichiometric or 10-fold molar excess of H_2O_2 (reaction cell concentrations). Spectral deconvolution was performed by global analysis and numerical integration methods using PROKIN software (Applied Photophysics Ltd.).

Oxidation of L-ascorbate by the W191F and N184R/W191F variants of C*c*P was measured using the sequential mixing mode of the stopped-flow apparatus: enzyme (4 μM) was mixed with H_2O_2 (6 μM) and the solution allowed to age for 20 ms (enabling formation of the porphyrin π-cation radical intermediate) prior to mixing with excess ascorbate. Oxidation of ascorbate was monitored at 423 nm at a range of substrate concentrations.

RESULTS AND DISCUSSION

Design of Site-Directed Variants. We noted originally (*1*) that a comparison of the C*c*P and APX structures in the region of the ascorbate binding site shows that the additional loop in C*c*P and the side chain of Tyr36 together prevent binding of ascorbate, and that Asn184 in C*c*P overlays with Arg172 in APX, Figure 1. In total 7 variants of C*c*P were therefore prepared with different combinations of the mutations Y36A, N184R and W191F. These were Y36A, N184R, W191F, N184R/W191F, Y36A/W191F, Y36A/N184R, and Y36A/N184R/W191F. The rationalization for the mutations was as follows: (i) Tyr36 directly blocks the equivalent ascorbate binding site in C*c*P and was therefore replaced with a less bulky residue; (ii) the N184R variant introduces

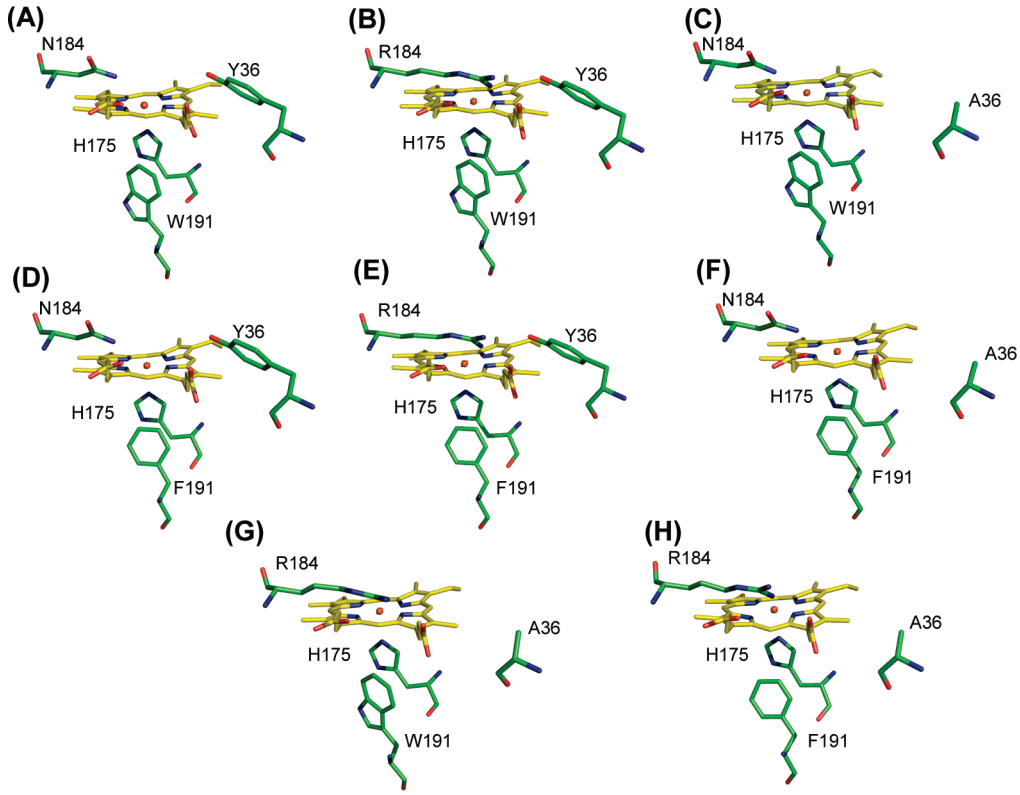

FIGURE 2: Structures of the C*c*P variants in the region of the heme. (A) Wild type C*c*P, (B) N184R, (C) Y36A, (D) W191F, (E) N184R/W191F, (F) Y36A/W191F, (G) Y36A/N184R and (H) Y36A/N184R/W191F. See also Figure S2 of the Supporting Information for electron densities. This figure was prepared using PyMol (*43*).

potential hydrogen bonding interactions for ascorbate binding; (iii) the W191F mutation was incorporated with the other mutations to assess whether C*c*P can support electron transfer directly through the heme edge, bypassing Trp191 (as in APX). Mutations that included a Lys in C*c*P were not included as part of this mutational analysis, because Lys 30, Figure 1, has been shown (*32*) to have little effect on ascorbate binding in APX.

Crystallographic Studies. We obtained structures for all of the variants presented in this paper, Table 2. The structures in the region of the heme are shown in Figure 2. In all cases, the structures were as expected and did not show major perturbations compared to the wild type protein (see also Figure S2 of the Supporting Information for electron densities).

Figure 3 shows the structure of the triple Y36A/N184R/W191F mutant close to the expected ascorbate binding site. The new variant, Figure 3(A), contains a cavity which was previously occupied by the side chain of Tyr36 and a single water molecule, Figure 3(C). Examination of the electron density in the new cavity, Figure 3(A), reveals two well-ordered water molecules which form hydrogen bonds to the engineered Arg184 residue and the heme 6-propionate. The first water molecule (labeled 1 in Figure 3(A)), is 2.70 Å from the O1 of the heme 6-propionate and 2.82 Å from the 1-NH group of Arg 184; the second is 2.82 Å from the 2-NH of Arg 184. Comparison of this structure with that of APX in the absence of ascorbate, Figure 3(B), shows that these water molecules in the triple C*c*P mutant are in analogous positions to two (also labeled 1 and 2 in Figure 3(B)) of the five water molecules seen in the ascorbate binding site of APX.

Crystal Structure of the Y36A/N184R/W191F−Ascorbate Complex. The structure of the Y36A/N184R/W191F triple mutant in complex with ascorbate is shown in Figure 3(D).[2] Comparison with the ascorbate-free structure shows that binding of ascorbate leads to no major structural rearrangements of the enzyme (data not shown). Ascorbate binds at the new cavity created at the γ-heme edge in place of the two water molecules seen in the unbound structure and in an analogous position to that observed for ascorbate bound to APX, Figure 3(A) (*10*). The refined atomic positions, Figure 3(D), show hydrogen bonds between the 2-OH (pK_a 4.0 (*31*)) of the substrate and the heme 6-propionate (2.6 Å) and from the 3-OH (pK_a 11.3 (*31*)) of the substrate and the 1-NH of Arg184 (2.4 Å). There are no clear hydrogen bonding interactions for the 6-OH group which is hydrogen bonded to Lys30 in APX; however, this interaction has been shown to have a minor role in stabilization of the substrate bound complex in APX (*32*). There is no evidence of ascorbate binding to any other site in the protein. By comparing the structure of the Y36A/N184R/W191F−ascorbate complex with that of the APX−ascorbate complex, Figure 3(E), it is clear that the ascorbate is orientated slightly differently in the two cases and that this affects the hydrogen bonding patterns. In the APX−ascorbate complex, Figure 3(E), the 2-OH group of the substrate makes two hydrogen bonds to the heme 6-propionate and Arg172; on the other hand, in the Y36A/N184R/W191F−ascorbate

[2] We have assigned the electron density as ascorbate since the enzyme has not been oxidized and therefore we assume that the substrate is not oxidized either. Note, however, that we are unable to distinguish between ascorbate and either of its oxidized products (monodehydroascorbate radical or dehydroascorbate).

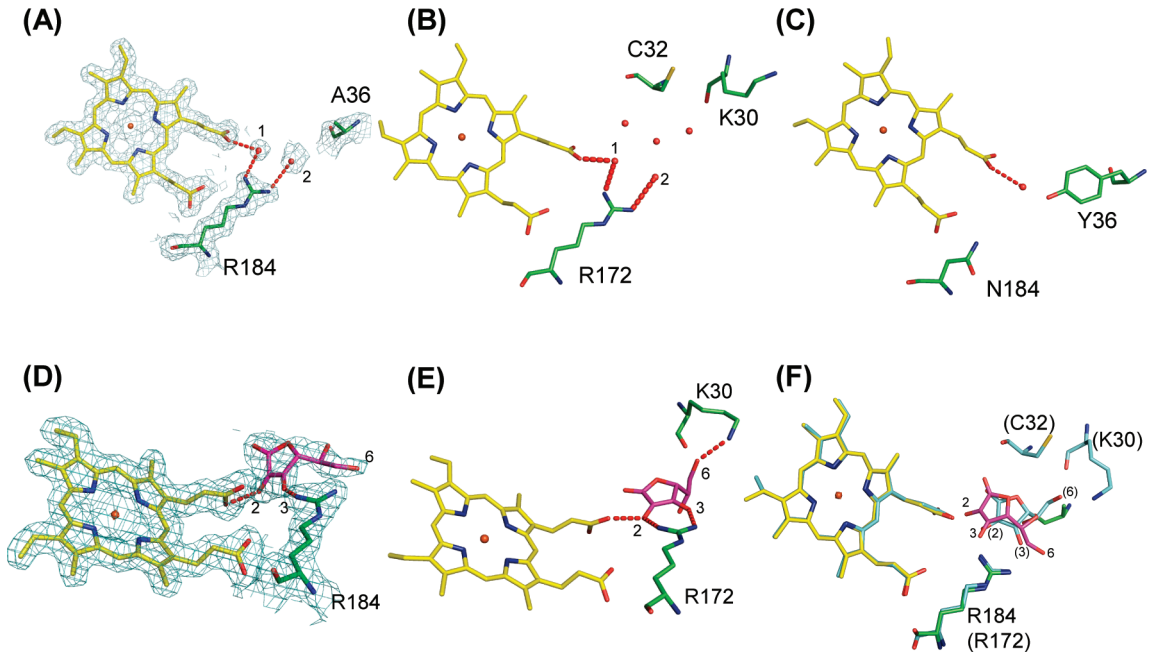

FIGURE 3: Comparison of the structures of the C*c*P variants with those of the APX−ascorbate complex. (A) The structure of Y36A/N184R/W191F. The F191 residue in the Y36A/N184R/W191F variant lies directly underneath the heme and is not shown in this orientation. In comparison to wild type C*c*P (C) two well ordered water molecules (labeled 1 and 2) occupy the new cavity created in similar positions to two of the water molecules (also labeled 1 and 2) seen in the ascorbate binding cavity of APX. (B), (C) The structures of wild type APX and C*c*P, respectively. (D) Refined electron density (aquamarine) for ascorbate (magenta) bound to the new cavity in Y36A/N184R/W191F (hydroxyl groups are labeled 2, 3 and 6). (E) The structure of the APX−ascorbate complex (*10*) (hydroxyl groups are as for (D)). (F) Comparison of the binding orientation for ascorbate in the APX−ascorbate complex (cyan) and Y36A/N184R/W191F (magenta). C*c*P residues are labeled with those for APX in parentheses and the hydroxyl groups of ascorbate are also labeled as in (E) and (F). In all figures, hydrogen bonds are indicated as red dotted lines and water molecules are shown as red spheres. This figure was prepared using PyMol (*43*).

complex, Figure 3(D), the altered binding orientation prevents the equivalent hydrogen bonding interaction between the 2-OH of the substrate and the 1-NH of Arg184. Equally, the 3-OH group of the substrate interacts with the 2-NH of Arg172 in APX, Figure 3(D), whereas this hydroxyl group interacts instead with the 1-NH group of Arg184 in the Y36A/N184R/W191F-ascorbate structure. A direct overlay of the APX-ascorbate complex and the Y36A/N184R/W191F-ascorbate complex is given in Figure 3(F).

Nature of the Reactive Intermediates. It was important to assess the nature of the intermediates formed during reaction of C*c*P and its variants with H_2O_2, so that the steady state data (*vide infra*) might be sensibly reconciled with the structural information. Reactions with H_2O_2 were examined by rapid scanning stopped-flow over a 500 ms time scale. For the wild type protein, addition of a stoichiometric amount of H_2O_2 leads to a red shift of the Soret band (from 410 to 421 nm) and the formation of two new bands at 533 and 562 nm, Figure 4(A), consistent with formation ($k_1 = 1 \times 10^7$ $M^{-1}s^{-1}$) of the expected Compound I species with a protein radical on Trp191.

The corresponding time-dependent spectroscopic changes for N184R and Y36A, under the same conditions, were similar to the wild type protein, Figures 4(B), (C) and we propose that formation ($k_1 = 1 \times 10^7$ $M^{-1}s^{-1}$ in both cases) of a normal Compound I with a radical on Trp191 occurs in these cases.

There are four variants which included the W191F mutation, and we wanted to assess whether a porphyrin π-cation radical was formed in these cases. For W191F and N184R/W191F this proved to be the case, because spectroscopic changes on reaction with H_2O_2 showed evidence for formation ($k_1 = 1.2 \times 10^6$ and 1.6×10^6 M^{-1} s^{-1}, respectively) of an initial intermediate ($\lambda_{max} = 412$, 543 and 656 nm in both cases), Figures 4(D), (E), which is consistent with a transient porphyrin π-cation radical, as observed previously for W191F (*33*). This intermediate is very unstable and decays over 500 ms in a first-order process ($k_2 \sim 20$ s^{-1} in both cases) to a final product ($\lambda_{max} = 423$, 535 and 565 nm) which is very similar to that of the wild type and is consistent with an oxy-ferryl species and a protein radical (*34*); since Trp191 is not available, the radical must reside on another residue, previously proposed as a tyrosine (*35*). For the Y36A/W191F variant, no significant spectroscopic changes on reaction with stoichiometric or higher amounts of H_2O_2, Figure 4(G), were seen. The Y36A/N184R variant, Figure 4(F), shows similar behavior, and this has been observed previously in other variants of C*c*P (*36, 37*).[3] As mentioned above, it is likely that nonspecific reactions, perhaps involving protein radical formation, occur in these cases, but this was not explored further.

In contrast to W191F and N184R/W191F, the Y36A/N184R/W191F variant shows no evidence for a porphyrin π-cation radical. In this case, reaction with peroxide is observed as for the wild type ($k_1 = 10^7$ M^{-1} s^{-1}). Since a porphyrin π-cation radical is clearly observed for Compound I species of the other variants containing the W191F mutation (W191F and N184R/W191F, above), we conclude that the formation of this species likely also occurs for Y36A/N184R/

[3] This variant also has a higher proportion of 6-coordinate heme in the ferric form, which may moderate reactivity.

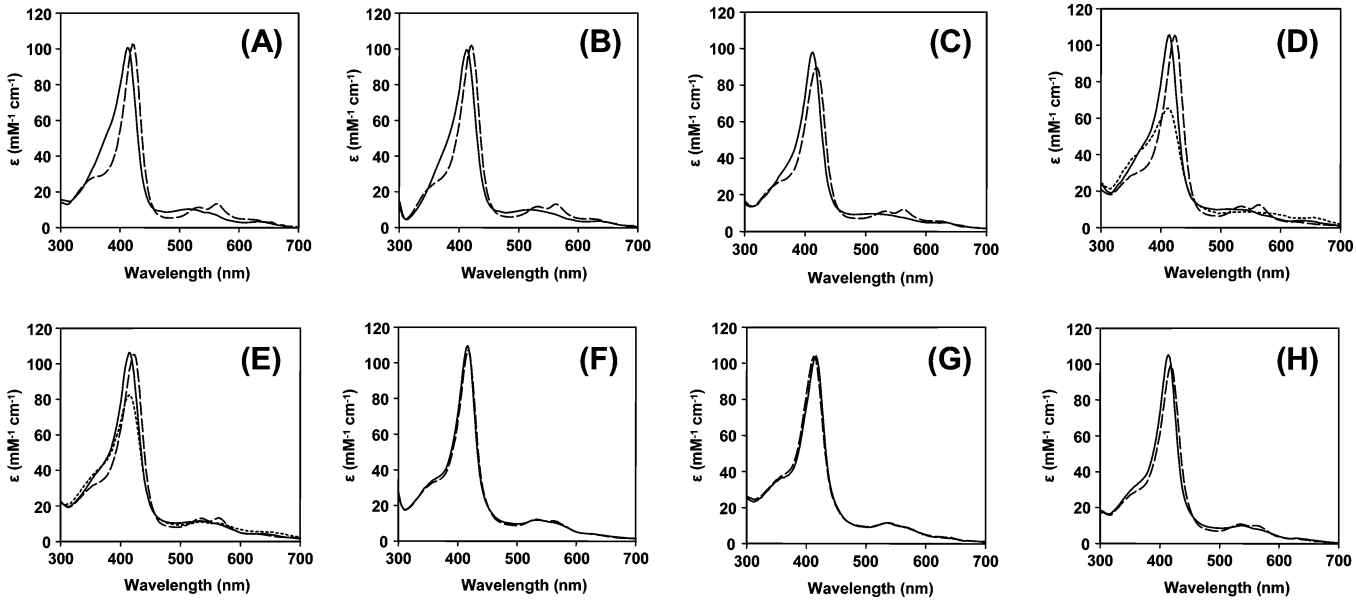

FIGURE 4: Photodiode array spectra for reaction of the C*c*P variants with H_2O_2. (A) Wild type C*c*P, (B) N184R, (C) Y36A, (D) W191F, (E) N184R/W191F, (F) Y36A/N184R, (G) Y36A/W191F and (H) Y36A/N184R/W191F. In each case the solid line indicates the spectrum before addition of H_2O_2 and the dashed line is after addition. Time-dependent changes were fitted either to an A → B model (panels (A), (B), (C), (F) and (H)) or an A → B → C model (panels (D), (E)); where intermediates were observed (panels (D), (E)), these are indicated by a dotted line. Enzyme was reacted stoichiometrically with H_2O_2, except for Y36A/W191F, panel (G), which was reacted with a 10-fold excess of H_2O_2.

Table 3: Kinetic Parameters for the Oxidation of Guaiacol Ascorbate and Cytochrome *c*[a]

	guaiacol		ascorbate		cytochrome *c*	
variant	k_{cat} (s^{-1})	K_M (mM)	k_{cat} (s^{-1})	K_M (mM)	k_{cat} (s^{-1})	K_M (μM)
wild type C*c*P	4.1 ± 0.3	53 ± 6.0	0.83 ± 0.14	0.71 ± 0.22	1510 ± 259	93 ± 31
N184R	3.0 ± 0.1	27 ± 1.6	1.5 ± 0.10	1.7 ± 0.21	570 ± 40	140 ± 18
Y36A	5.4 ± 0.2	36 ± 3.1	1.3 ± 0.08	1.7 ± 0.19	580 ± 35	230 ± 28
W191F	14 ± 0.6	57 ± 4.6	0.25 ± 0.01	0.45 ± 0.004	1.7 ± 0.13	100 ± 16
N184R/W191F	4.9 ± 0.2	34 ± 2.2	0.27 ± 0.01	0.31 ± 0.004	0.08 ± 0.01	670 ± 110
Y36A/W191F	3.2 ± 0.2	45 ± 2.5	0.45 ± 0.06	0.50 ± 0.13	0.06 ± 0.01	160 ± 17
Y36A/N184R	0.9 ± 0.01	16 ± 0.7	0.66 ± 0.03	0.48 ± 0.06	600 ± 27	110 ± 10
Y36A/N184R/W191F	1.5 ± 0.1	14 ± 1.2	2.6 ± 0.35	1.3 ± 0.22	1.6 ± 0.13	300 ± 27

[a] All assays were carried out in 0.1 M KPi buffer at pH 6.0 and 25 °C.

W191F but that the introduction of the Y36A mutation destabilizes the porphyrin π-cation radical such that it decays on a time scale that is too rapid for the stopped-flow experiment. This is consistent with the data for Y36A/W191F (above), which also show no evidence for a porphyrin π-cation intermediate.

Steady-State Oxidation of Substrates. The competency of the variants to support oxidation of various substrates was assessed in parallel steady state assays. Table 3 shows data for oxidation of guaiacol, ascorbate and cytochrome *c*. We use this information to make correlations with the pre-steady data above.

As expected (*15, 33*), the W191F mutation dramatically reduced the activity toward cytochrome *c*, but in the other variants which did not contain the W191F mutation the activity toward cytochrome *c* was largely unaffected, Table 3.

Guaiacol oxidation was not significantly affected by any of the mutations, including W191F, which is consistent with the idea that aromatic substrates such as guaiacol bind at a separate location close to the δ-heme edge (*1, 38*) and is clearly indicative of a different electron transfer pathway for the oxidation of these types of aromatic substrate.

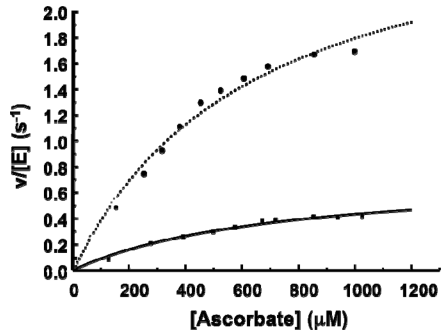

FIGURE 5: Steady-state oxidation of L-ascorbate by C*c*P. Wild type C*c*P (solid line) and Y36A/N184R/W191F (dashed line) (0.1 M potassium phosphate, pH 6.0, 25 °C). The solid lines are a fit to the Michaelis−Menten equation.

Ascorbate oxidation is measurable but slow for wild type C*c*P, with clear changes in absorbance at 290 nm which report directly on ascorbate oxidation (as in APX (*26*)). We determine $k_{cat} = 0.83 \pm 0.14\ s^{-1}$ for the wild type enzyme, Figure 5, which compares with a previous value of 3 s^{-1} (*39*). We also clearly observe oxidation of ascorbate for all the variants, Table 3 and Figure 5. On the whole, however, the rates of oxidation are not markedly increased from those

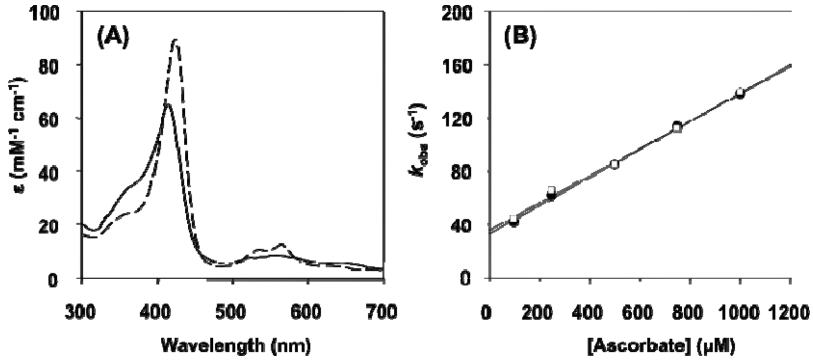

FIGURE 6: Oxidation of ascorbate by the transient porphyrin π-cation intermediate. (A) Deconvoluted spectra for the reaction of the porphyrin π-cation intermediate in W191F with ascorbate. The solid line indicates the porphyrin π-cation intermediate formed after mixing enzyme with H_2O_2; the dashed line is the final species after addition of ascorbate to the first intermediate. Similar spectra were observed for W191F/N184R (not shown). (B) Dependence of the observed rate constant, k_{obs}, for reduction of the porphyrin π-cation intermediate on ascorbate concentration for W191F (filled circles) and N184R/W191F (open squares). Conditions: [enzyme] = 4 μM, [H_2O_2] = 6 μM (both cell concentrations), 0.1 M potassium phosphate, pH 6.0; delay time of 20 ms before reaction with ascorbate contained in the same buffer.

of wild type C*c*P, with the highest value of k_{cat} observed for the Y36A/N184R/W191F variant (k_{cat} = 2.6 ± 0.35 s^{-1}, Figure 5).

Together, these kinetic data allow us to make useful comparisons between APX and C*c*P. Hence, although W191F and N184R/W191F (and, we assume, Y36A/N184R/W191F) clearly forms a porphyrin π-cation radical as for APX (above), the formation of this intermediate does not translate into high ascorbate activity in the steady state. We conclude that in the C*c*P variants the decay of the essential porphyrin π-cation species is much too rapid ($k_1 \approx 20$ s^{-1} compared to ≈ 0.03 s^{-1} for APX) to support oxidation of the substrate ($k_{cat} \approx 1$ s^{-1} compared to ≈ 80 s^{-1} for APX) in the steady state.

Reactivity of the Porphyrin π-Cation Intermediate with Ascorbate. The above data raise the question about the inherent reactivity of the porphyrin π-cation intermediate, and whether it may, in fact, be competent for ascorbate oxidation under different conditions where its rapid decay was not competitive with substrate oxidation (i.e., in the pre-steady state).

To assess this, we carried out double mixing experiments with W191F, Figure 6, and N184R/W191F (data not shown) in the presence of H_2O_2 and ascorbate. Initial formation of the transient porphyrin π-cation intermediate was observed (as above) on reaction of both ferric enzymes with H_2O_2. On addition of ascorbate in a second mixing event, we then observe that conversion to the final product (i.e., B → C) occurred much more rapidly than in the absence of ascorbate, Figure 6.[4] There is a linear dependence of the observed rate constants on ascorbate concentration (data not shown), from which a second order rate constant $k_{on} \sim 1.0 \times 10^5$ M^{-1} s^{-1} can be derived in both cases; this linear dependence also shows an intercept, $k_{off} \approx 34$ s^{-1}, which most likely reflects decay of the intermediate (with k_{off} approximately the same as that measured above (≈20 s^{-1})).[5] A direct comparison with wild type C*c*P is not possible, see footnote 6, but it is possible to compare the second order rate constant measured above with that for reduction of Compound I by ascorbate in horseradish peroxidase (HRP). For HRP, a rate constant of 1.8×10^5 M^{-1} s^{-1} is reported (*44*), which compares well with our value above.

These data highlight two important points. First, they show that in cases where a porphyrin π-cation intermediate forms it is indeed capable of ascorbate oxidation, but that its decay under steady state conditions occurs much too rapidly for efficient turnover. This presumably means that the porphyrin π-cation intermediate is competent for electron transfer, in the sense that it can be reduced by substrate in a step that requires only electron transfer (and not proton transfer, see below). Second, since the on rate constants in the presteady state experiments ($k_{on,obs} \approx 40-120$ s^{-1}) are much faster than our measured values for k_{cat} in the steady state, substrate binding is not likely to be limiting in the steady state, and we conclude that some other process (e.g., proton transfer during reduction of Compound II) controls turnover. This would explain why the k_{cat} values are broadly similar in all variants.[6]

Implications for Substrate Binding in Other Heme Enzymes. Our appreciation of the substrate binding specificities across a range of heme proteins has changed as we have learned that different heme enzymes can bind and oxidize different substrates at different sites. Although C*c*P has an anomalous substrate, we have recently shown (*38*) that C*c*P binds the aromatic substrate isoniazid at the δ-heme edge. In this sense, C*c*P is behaving more conventionally insofar

[4] In contrast, in experiments with Y36A/N184R/W191F and wild type protein, neither of which forms a porphyrin π-cation radical, there were no changes to the transients in the presence of ascorbate (compared to those in the absence of ascorbate, Figure 4).

[5] The corresponding reaction of C*c*P with ascorbate was also examined in control reactions. (This does not provide a direct comparison, however, because the structure of the Compound I intermediate for the wild type protein (Trp radical) is different from that in W191F and N184R/W191F.) In this experiment, stoichiometric addition of H_2O_2 led to formation of the expected Compound I, but on addition of ascorbate very small changes in spectra were observed over 1 s that most likely represent reduction to Compound II (i.e., reduction of the protein radical occurs). Over longer time scales (60 s), reduction back to ferric heme is observed, which is consistent with the steady state data.

[6] We cannot rule out a further possibility that the ascorbate site seen in our structure is not the site of oxidation, and that a second ascorbate site exists. We consider this unlikely because our other structural work on both APX and C*c*P (in the presence of high concentrations of ascorbate) has never revealed a second binding site. We note, however, that in lignin peroxidase two binding sites for substrate have been proposed (Choinowski, T., Blodig, W., and Winterhalter, K. (1999) *J. Mol. Biol. 286*, 809−827; Blodig, W., Smith, A. T., Doyle, W., Piontek, K. (2001) *J. Mol. Biol. 305*, 851−861).

as it is binding a substrate and oxidizing it at the δ-heme edge as observed for other peroxidase enzymes. This must mean that a separate conduit for electron transfer, independent of that used for oxidation of cytochrome *c*, must be available, and our steady state data for oxidation of guaiacol support this.

But it is now clear that the δ-heme edge does not have a monopoly on substrate oxidation, and that the γ-heme edge is also important. There are three examples: the manganese peroxidase/Mn(II) complex (*9*), the nitric oxide synthase/tetrahydrobiopterin complex (*12*) and the APX/ascorbate complex (*10*). In all three cases, the heme propionate is involved in a hydrogen-bonding interaction with the bound substrate (although it is not the same propionate in all cases) and the role of these propionate groups as direct participants in the catalytic process has recently attracted attention (*40*−*42*). The data presented here now show that this same binding interaction can also be engineered in C*c*P. Hence, we have shown that relatively minor alterations in structure at Tyr36 and Asn184 are enough to allow ascorbate to bind to C*c*P at the γ-heme edge in the same site and with essentially the same hydrogen bonding pattern as that observed for APX. Although we only have a structure for the triple variant, we suggest that binding, albeit weakly, most likely occurs at this same site in the other variants and possibly even in the wild type protein.

Our data also show that C*c*P is functionally competent for oxidation of the ascorbate in the engineered variants, but there is little real enhancement of activity over the latent activity of the wild type enzyme in this or any of the other variants studied in the steady state. In this sense, the steady state turnover certainly does not approach that observed in APX ($k_{cat} \approx 80\ s^{-1}$) even in the Y36A/N184R/W191F variant. The pre-steady state data for W191F and N184R/W191F demonstrate an intrinsic competency of the porphyrin π-cation radical in Compound I for ascorbate oxidation, as a simple electron transfer process. This is not, however, enough to support steady state turnover because the decay of the transient porphyrin π-cation radical outruns ascorbate oxidation. This is in contrast to the situation in APX, where decay of Compound I is much slower and not competitive with steady state turnover. In fact, even if the decay of the porphyrin π-cation intermediate were not so rapid, it is likely that proton transfer during reduction of Compound II by ascorbate would be rate limiting during turnover (as is the case for APX) so that the straightforward introduction of a substrate binding site would need also to be coupled to proton delivery.

It appears, therefore, that the combination of efficient substrate binding, together with the formation of a suitably stable porphyrin π-cation radical, seems to be the key to rapid substrate oxidation at the γ-heme edge (and, indeed, the δ-heme edge) and that hydrogen bonding plays a crucial role. The wider role of the heme propionates should also not be underestimated: it may well be the case that, in addition to providing glue for substrate binding, these charged groups have other, as yet unidentified, biological roles.

ACKNOWLEDGMENT

We thank Grant Mauk for the gift of the C*c*P expression vector and Dr Igor Efimov for helpful discussions. We are also grateful to an anonymous reviewer for insightful comments on the kinetic data.

NOTE ADDED DURING REVIEW

While this paper was under review, another paper appeared (Meharenna et al. (2008) *Biochemistry 47,* 10324−10332), based on the APX-ascorbate structure (*10*), in which C*c*P was also engineered to encourage ascorbate binding. In this paper, the LREDDEYDNYIGY loop, Figure 1, was replaced with the corresponding APX sequence (IAEKKC) and coupled with the N184R and W191F mutations. Crystal structures are presented but none have ascorbate bound to the enzyme. Molecular dynamics calculations indicate that Asn80 allows movement of the ascorbate and thus prevents ascorbate binding. These calculations are not consistent with our crystallographic data for the ascorbate-bound complex of Y36A/N184R/W191F, Figure 3(D), since the same Asn (Asn87) is present and cannot, therefore, prevent binding of ascorbate. In addition, the Meharenna et al. paper reports an enhancement of ascorbate activity ($k_{cat} = 12\ min^{-1}$) for the best mutant, but this is based on a complete absence of ascorbate activity for wild type C*c*P, whereas we and others ($\approx 1\ s^{-1}$, Table 1, and $\approx 3\ s^{-1}$ (*39*), respectively) observe clear activity for wild type C*c*P at greater than $12\ min^{-1}$.

SUPPORTING INFORMATION AVAILABLE

Electronic spectra and structures for the variants, plus electron density for the ascorbate site. This material is available free of charge via the Internet at http://pubs.acs.org.

REFERENCES

1. Sharp, K. H., Moody, P. C. E., Brown, K. A., and Raven, E. L. (2004) Crystal structure of the ascorbate peroxidase-salicylhydroxamic acid complex. *Biochemistry 43*, 8644–8651.
2. Henriksen, A., Schuller, D. J., Meno, K., Welinder, K. G., Smith, A. T., and Gajhede, M. (1998) Structural interactions between horseradish peroxidase C and the substrate benzhydroxamic acid determined by x-ray crystallography. *Biochemistry 37*, 8054–8060.
3. Itakura, H., Oda, Y., and Fukuyama, K. (1997) Binding mode of benzhydroxamic acid to arthromyces ramosus peroxidase shown by X-ray crystallographic analysis of the complex at 1.6 angstrom resolution. *FEBS Lett. 412*, 107–110.
4. Tsukamoto, K., Itakura, H., Sato, K., Fukuyama, K., Miura, S., Takahashi, S., Ikezawa, H., and Hosoya, T. (1999) Binding of salicylhydroxamic acid and several aromatic donor molecules to *Arthromyces ramosus* peroxidase, investigated by X-ray crystallography, optical difference spectroscopy, NMR relaxation, molecular dynamics, and kinetics. *Biochemistry 38*, 12558–12568.
5. Henriksen, A., Smith, A. T., and Gajhede, M. (1999) The structures of the horseradish peroxidase C-ferulic acid complex and the ternary complex with cyanide suggest how peroxidases oxidize small phenolic substrates. *J. Biol. Chem. 274*, 35005–35011.
6. DePillis, G. D., Sishta, B. P., Mauk, A. G., and de Montellano, P. R. O. (1991) Small substrates and cytochrome-*c* are oxidized at different sites of cytochrome-*c* peroxidase. *J. Biol. Chem. 266*, 19334–19341.
7. Ator, M. A., David, S. K., and de Montellano, P. R. O. (1987) Structure and catalytic mechanism of horseradish-peroxidase - regiospecific meso-alkylation of the prosthetic heme group by alkylhydrazines. *J. Biol. Chem. 262*, 14954–14960.
8. Ator, M. A., and de Montellano, P. R. O. (1987) Structure and catalytic mechanism of horseradish peroxidase. *J. Biol. Chem. 262*, 1542–1551.
9. Sundaramoorthy, M., Kishi, K., Gold, M. H., and Poulos, T. L. (1994) The crystal structure of manganase peroxidase from *Phanerochaete crysosporium* at 2.06 Å resolution. *J. Biol. Chem. 269*, 32759–32767.

10. Sharp, K. H., Mewies, M., Moody, P. C. E., and Raven, E. L. (2003) Crystal structure of the ascorbate peroxidase−ascorbate complex. *Nat. Struct. Biol. 10*, 303–307.
11. Wei, C. C., Crane, B. R., and Stuehr, D. J. (2003) Tetrahydrobiopterin radical enzymology. *Chem. Rev. 103*, 2365–2383.
12. Poulos, T. L., Li, H. Y., Raman, C. S., and Schuller, D. J. (2001) Structures of gas-generating heme enzymes: nitric oxide synthase and heme oxygenase. *Adv. Inorg. Chem. 51*, 243–293.
13. Pelletier, H., and Kraut, J. (1992) Crystal-structure of a complex between electron-transfer partners, cytochrome-*c* peroxidase and cytochrome-*c*. *Science 258*, 1748–1755.
14. Bonagura, C. A., Sundaramoorthy, M., Pappa, H. S., Patterson, W. R., and Poulos, T. L. (1996) An engineered cation site in cytochrome *c* peroxidase alters the reactivity of the redox active tryptophan. *Biochemistry 35*, 6107–6115.
15. Mauro, J. M., Fishel, L. A., Hazzard, J. T., Meyer, T. E., Tollin, G., Cusanovich, M. A., and Kraut, J. (1988) Tryptophan-191-phenylalanine, a proximal-side mutation in yeast cytochrome-*c* peroxidase that strongly affects the kinetics of ferrocytochrome-*c* oxidation. *Biochemistry 27*, 6243–6256.
16. Nelson, D. P., and Kiesow, L. A. (1972) Enthalpy of decomposition of hydrogen peroxide by catalase at 25 degrees C (with molar extinction coefficients of H_2O_2 solutions in the UV). *Anal. Biochem. 49*, 474–478.
17. Metcalfe, C. L., Ott, M., Patel, N., Singh, K., Mistry, S. C., Goff, H. M., and Raven, E. L. (2004) Autocatalytic formation of green heme: Evidence for H_2O_2-dependent formation of a covalent methionine-heme linkage in ascorbate peroxidase. *J. Am. Chem. Soc. 126*, 16242–16248.
18. Fishel, L. A., Villafranca, J. E., Mauro, J. M., and Kraut, J. (1987) Yeast cytochrome-*c* peroxidase - mutagenesis and expression in escherichia-coli show tryptophan-51 is not the radical site in compound-I. *Biochemistry 26*, 351–360.
19. Antonini, M., and Brunori, E. (1971) *Hemoglobin and myoglobin and their reactions with ligands*, North Holland Publishers, Amsterdam, p 10.
20. Pond, A. E., Sono, M., Elenkova, E. A., Goodin, D. B., English, A. M., and Dawson, J. H. (1999) Influence of protein environment on magnetic circular dichroism spectral properties of ferric and ferrous ligand complexes of yeast cytochrome *c* peroxidase. *Biospectroscopy 5*, S42−S52.
21. Leslie, A. G. W. (1992) Joint CCP4 + ESF-EAMCB newsletter on protein crystallography. No. *26*.
22. Bailey, S. (1994) The CCP4 suite - programs for protein crystallography. *Acta Crystallogr., Sect D: Biol. Crystallogr. 50*, 760–763.
23. Finzel, B. C., Poulos, T. L., and Kraut, J. (1984) Crystal-structure of yeast cytochrome-*c* peroxidase refined at 1.7 A resolution. *J. Biol. Chem. 259*, 3027–3036.
24. Murshudov, G. N., Vagin, A. A., and Dodson, E. J. (1997) Refinement of macromolecular structures by the maximum-likelihood method. *Acta Crystallogr., Sect. D: Biol. Crystallogr. 53*, 240–255.
25. Emsley, P., and Cowtan, K. (2004) Coot: Model-building tools for molecular graphics. *Acta Crystallogr., Sect. D: Biol. Crystallogr. 60*, 2126–2132.
26. Lad, L., Mewies, M., and Raven, E. L. (2002) Substrate binding and catalytic mechanism in ascorbate peroxidase: Evidence for two ascorbate binding sites. *Biochemistry 41*, 13774–13781.
27. Kang, D. S., and Erman, J. E. (1982) The cytochrome-*c* peroxidase-catalyzed oxidation of ferrocytochrome-*c* by hydrogen-peroxide - steady-state kinetic mechanism. *J. Biol. Chem. 257*, 2775–2779.
28. Lad, L., Mewies, M., Basran, J., Scrutton, N. S., and Raven, E. L. (2002) Role of histidine 42 in ascorbate peroxidase - kinetic analysis of the H42A and H42E variants. *Eur. J. Biochem. 269*, 3182–3192.
29. Asada, K. (1984) Chloroplasts - formation of active oxygen and its scavenging. *Methods Enzymol. 105*, 422–427.
30. Santimone, M. (1975) Titration study of guaiacol oxidation by horseradish-peroxidase. *Can. J. Biochem. 53*, 649–657.
31. Bryan, D. M., Pell, S. D., Kumar, R., Clarke, M. J., Rodriguez, V., Sherban, M., and Charkoudian, J. (1988) Stable pentaamminеruthenium(III) complexes of reductic acids - synthesis, linkage isomers, and autoxidation kinetics. *J. Am. Chem. Soc. 110*, 1498–1506.
32. Macdonald, I. K., Badyal, S. K., Ghamsari, L., Moody, P. C. E., and Raven, E. L. (2006) Interaction of ascorbate peroxidase with substrates: A mechanistic and structural analysis. *Biochemistry 45*, 7808–7817.
33. Miller, M. A., Vitello, L., and Erman, J. E. (1995) Regulation of interprotein electron-transfer by Trp-191 of cytochrome-*c* peroxidase. *Biochemistry 34*, 12048–12058.
34. Hoffman, B. M., Roberts, J. E., Kang, C. H., and Margoliash, E. (1981) Electron-paramagnetic and electron nuclear double-resonance of the hydrogen-peroxide compound of cytochrome-*c* peroxidase. *J. Biol. Chem. 256*, 6556–6564.
35. Scholes, C. P., Liu, Y. J., Fishel, L. A., Farnum, M. F., Mauro, J. M., and Kraut, J. (1989) Recent endor and pulsed electron-paramagnetic resonance studies of cytochrome-*c* peroxidase - compound-I and its site-directed mutants. *Isr. J. Chem. 29*, 85–92.
36. Pearl, N. M., Jacobson, T., Arisa, M., Vitello, L. B., and Erman, J. E. (2007) Effect of single-site charge-reversal mutations on the catalytic properties of yeast cytochrome *c* peroxidase: Mutations near the high-affinity cytochrome c binding site. *Biochemistry 46*, 8263–8272.
37. Vitello, L. B., Erman, J. E., Miller, M. A., Mauro, J. M., and Kraut, J. (1992) Effect of Asp235Asn substitution on the absorption-spectrum and hydrogen-peroxide reactivity of cytochrome-*c* peroxidase. *Biochemistry 31*, 11524–11535.
38. Metcalfe, C., Macdonald, I. K., Murphy, E. J., Brown, K. A., Raven, E. L., and Moody, P. C. E. (2008) The tuberculosis prodrug isoniazid bound to activating peroxidases. *J. Biol. Chem. 283*, 6193–6200.
39. Yonetani, T., and Ray, G. S. (1965) Studies on cytochrome *c* peroxidase: Purification and some properties. *J. Biol. Chem. 240*, 4503–4514.
40. Poulos, T. L. (2007) The Janus nature of heme. *Nat. Prod. Rep. 24*, 504–510.
41. Schoneboom, J. C., Cohen, S., Lin, H., Shaik, S., and Thiel, W. (2004) Quantum mechanical/molecular mechanical investigation of the mechanism of C-H hydroxylation of camphor by cytochrome P450(cam): Theory supports a two-state rebound mechanism. *J. Am. Chem. Soc. 126*, 4017–4034.
42. Guallar, V., Baik, M. H., Lippard, S. J., and Friesner, R. A. (2003) Peripheral heme substituents control the hydrogen-atom abstraction chemistry in cytochromes P450. *Proc. Natl. Acad. Sci. U.S.A. 100*, 6998–7002.
43. DeLano, W. L. (2002) DeLano Scientific, San Carlos, CA.
44. Lambier, A.-M., Dunford, H. B., and Pickard, M. A. (1987) Kinetics of the oxidation of ascorbic acid, ferrocyanide and p-phenolsulfonic acid by chloroperoxidase Compounds I and II. *Eur. J. Biochem. 163*, 123–127.

BI801480R